BIOCHEMISTRY
including biophysical chemistry & molecular biology
Article

Biochemistry **2011,** *50,* 1255–1264 1255
DOI: 10.1021/bi101650q

Structure of *Ralstonia eutropha* Flavohemoglobin in Complex with Three Antibiotic Azole Compounds†

Emna El Hammi,‡,∥ Eberhard Warkentin,§ Ulrike Demmer,§ Férid Limam,⊥ Nejib M. Marzouki,∥ Ulrich Ermler,§ and Laura Baciou*,‡

‡*Laboratoire de Chimie Physique, CNRS-Université Paris-Sud 11, UMR8000, F-91405 Orsay, France,* §*Max-Planck-Institut für Biophysik, Frankfurt, Germany,* ∥*UGB 99UR09-26 INSAT, University of 7 November at Carthage, Tunisia, and* ⊥*Laboratoire Interactions Légumineuses Microorganismes, CBBC, Hammam-Lif, Tunisia*

Received October 14, 2010; Revised Manuscript Received December 28, 2010

ABSTRACT: Flavohemoglobins (flavoHbs) are enzymes that operate primarily as nitric oxide dioxygenases and shuttle thereby electrons among NAD(P)H, FAD, heme, and a ligated redox-active substrate such as O_2. They function in the bacterial defense against nitrosative stress and are therefore considered as targets for new antibiotic drugs. Recently, azole derivatives were proven to be attractive nitric oxide dioxygenase inhibitors, and to explore their binding characteristics, we determined the X-ray structure of the flavoHb from *Ralstonia eutropha* in a complex with miconazole (FHP_M), econazole (FHP_E), and ketoconazole (FHP_K). In agreement with UV−vis spectroscopic data, one azole compound binds inside the distal heme pocket and ligates to the heme iron by its imidazole substituent. The two additional substituents, mostly chlorinated phenyl groups, form a series of van der Waals contacts with the protein matrix. Both interactions explain their high affinity for flavoHbs, the binding constants being 2.6, 1.2, and 11.6 μM for miconazole, econazole, and ketoconazole, respectively. The FHP_M and FHP_{Lip} (flavoHbs originally loaded with a phospholipid) structures share an "open" state and the FHP_E and FHP_K structures a "closed" state. Although the azole compounds were able to push the lipid out of its binding site, a fatty acid fragment is still bound inside the heme pocket of FHP_E and FHP_K and dictates the state of the protein. The ligand-induced open-to-closed transition involves a reorientation of the NADH domain accompanied by conformational changes in the C-terminal arm, helix E, and the CE loop resulting in an encapsulation of the heme-binding pocket. Implications of the observed open-to-closed process on the catalytic cycle are discussed.

Flavohemoglobins (flavoHbs)[1] have been discovered in a wide variety of microbes (prokaryotic and eukaryotic), where they play a key role in the complex cell response to nitrosative stress (*1*). Architecturally, they consist of an N-terminal heme *b* binding globin module and a C-terminal FAD-dependent ferredoxin $NAD(P)^+$ reductase-like module composed of a FAD and NADH binding domain. The two fused modules create a NADH-dependent oxidoreductase of ca. 43 kDa where the flavin serves as a transformer between the two-electron carrier NAD^+/NADH and the one-electron carrier heme *b*, which ligates the redox-active substrate. FlavoHbs from diverse organisms share a sequence identity beyond 30% and were subjected to diverse structural and functional investigations (*1*−*4*). X-ray structures were determined for the *Ralstonia eutropha* (PDB entry 1CQX) (*5*) and the highly homologous *Escherichia coli* flavoHbs (PDB entry 1GVH) (*6*). X-ray structures of both proteins are mainly distinguished by different orientations of the NADH relative to the FAD and heme domains and of helix E that determine the size of the distal heme pocket. Whereas the *R. eutropha* enzyme contained phosphatidylethanolamine (major compound) or phosphatidylglycerol (therefore termed FHP_{Lip}) (*7*), the *E. coli* flavoHb (termed HMP) was structurally characterized in a phospholipid-free form. However, HMP and the globin homologue from *Vitreoscilla* are able to bind reversibly phospholipids in solution (*6*, *8*), reflecting the high degree of conservation of the lipid binding region (*9*).

The physiological role of microbial flavoHbs has not been ultimately elucidated, although their crucial function in NO detoxification and in NO signaling modulation (via NorR, NsrR, and FNR) is well established (in vitro and in vivo) in organisms like *E. coli* and *R. eutropha* (*1*−*3*, *10*−*12*). NO is released by macrophages and other immune cells of animals and plants to repel an attack of (pathogenic) microorganisma. FlavoHbs most efficiently function as nitric oxide dioxygenases (NOD), which convert NO and O_2 to nitrate (*13*−*16*). Moreover, microbial NODs regulate their own expression by responding to the NO level (*17*). It was shown, in addition, that microbial flavoHbs have an NO reductase (*18*) and an alkylhydroperoxidase reductase (*2*, *19*) activity under anaerobic conditions. Their protective role against nitrosative stress makes microbial flavohemoglobins attractive as targets for antibiotic design. Recent studies have demonstrated that azole derivatives like miconazole, econazole,

†This work was supported by a collaborative French and Tunisian grant (PHC-CMCU Utique 08G0801).

*To whom correspondence should be addressed: Laboratoire de Chimie Physique, CNRS-Université Paris-Sud 11, F-91405 Orsay, France. Phone: +33 (0) 1 69 15 77 11. Fax: +33 (0) 1 69 15 61 88. E-mail: Laura.baciou@u-psud.fr.

[1]Abbreviations: flavoHb, flavohemoglobin; FHP_{Lip}, FHP_M, FHP_E, and FHP_K, flavohemoglobin from *Ralstonia eutropha* in a complex with lipid, miconazole, econazole, and ketoconazole, respectively; HMP, flavohemoglobin from *Escherichia coli*; PDB, Protein Data Bank; rms, root-mean-square.

Published on Web 01/06/2011

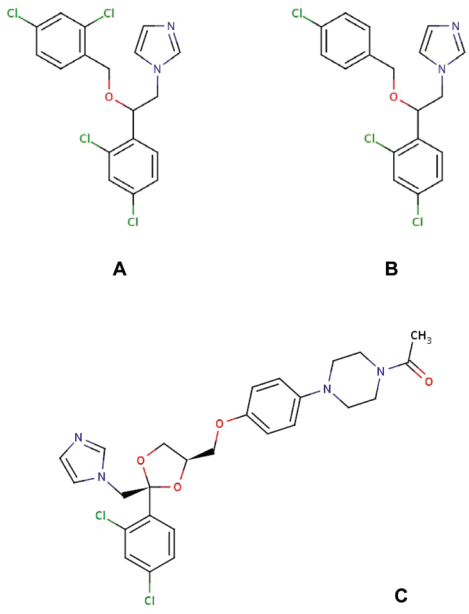

FIGURE 1: Structural formulas of miconazole, econazole, and ketoconazole (*46*, *47*). (A) Miconazole, 1-{2-(2,4-dichlorophenyl)-2-[(2,4-dichlorophenyl)methoxy]ethyl}imidazole ($C_{18}H_{14}Cl_4N_2O$) (M_r = 416.12 kDa). For the sake of description, miconazole is subdivided into dichlorobenzyl, dichlorophenylmethoxy, and methylimidazol moieties covalently linked to a central carbon atom. (B) Econazole, 1-{2-[(4-chlorophenyl)methoxy]-2-(2,4-dichlorophenyl)ethyl}imidazole ($C_{18}H_{15}Cl_3N_2O$) (M_r = 381.68 kDa). (C) Ketoconazole, 1-[4-(4-{[(2*S*,4*R*)-2-(2,4-dichlorophenyl)-2-(imidazol-1-ylmethyl)-1,3-dioxolan-4-yl]methoxy} phenyl)piperazin-1-yl]ethanone ($C_{26}H_{28}Cl_2N_4O_4$) (M_r = 531.43 kDa).

and ketoconazole (Figure 1) inhibit the NOD activity of microbial flavoHbs (*20*). The inhibition constants (K_i) range from a few to several thousand nanomolar depending on the organism and the type of azole derivative. According to spectroscopic analysis, the imidazole nitrogen seems to coordinate to the ferric heme iron. In vivo studies substantiate their antimicrobial effect in *Staphylococcus aureus* as cells expressing FlavoHb contain larger amounts of reactive oxygen species in the presence of azole compounds (*21*). Azole derivatives have been used for many years in the treatment of fungal infections and are essentially targeted against cytochrome P450 enzymes (*22*) through heme coordination (*23*−*26*). For example, econazole is a topical treatment for yeast and fungal infections and was effective in clearing *Mycobacterium tuberculosis* from infected mice (*27*).

The binding of individual azole derivatives to bacterial flavoHbs has been explored only on the basis of spectral and kinetic data. No crystal structure of the antibiotic azole compound bound in any FlavoHb active site has been reported. The available *E. coli* and *R. eutropha* flavoHb structures are drastically different with respect to the distal heme pocket, the potential azole binding site, and thus do not provide a serious structural basis for understanding azole binding. In this report, the X-ray structure of flavoHbs from *R. eutropha* was determined in complex with miconazole (FHP_M), ketoconazole (FHP_K), and econazole (FHP_E) at 2.0, 2.3, and 2.4 Å resolution, respectively. Accordingly, we describe the interactions between the protein matrix and the three inhibitors in a comparative manner and how the bulky structures of the azole inhibitors dictate the profile of the heme-binding pocket and vice versa in flavoHbs. Finally, the impact of the structural data for the catalytic reaction and the potential of the distal heme pocket for future drug design are discussed.

MATERIALS AND METHODS

Protein Expression and Purification. FlavoHb of *R. eutropha* was expressed in *E. coli* BL21 strains and purified as described previously (*28*), with few modifications. After sonication, the soluble fraction of the cell extract was precipitated with 25% ammonium sulfate, dialyzed, and then loaded onto a DEAE Sepharose anion-exchange column equilibrated with 20 mM potassium phosphate (pH 7.5). Bound proteins were eluted with a linear gradient between 0 and 30% KCl (1 M). Fractions with an A_{280}/A_{395} ratio of <1.0 were pooled, concentrated, and further separated using the Superdex 75 gel filtration column equilibrated with 20 mM potassium phosphate (pH 7.5) and 10 mM KCl (buffer A). Purity was analyzed via 10% bistris Nupage SDS gel electrophoresis (Invitrogen) and stained with Coomassie Brilliant Blue. Protein concentrations were determined with the Bradford method and spectrophotometrically at the Soret maximum of heme with an ε_{395} of 123000 M^{-1} cm^{-1}.

Ligand Binding Studies. Binding of miconazole, econazole, and ketoconazole to purified flavoHb was examined by monitoring the concentration-dependent increase in the level of the high-spin form of the enzyme by visible absorption spectroscopy. All reagents were purchased from Sigma Aldrich unless specifically mentioned. Absorption spectra were recorded on a double-beam Uvikon 943 spectrophotometer (Kontron Instruments) using a 1.0 cm light path quartz cuvette at 21 °C. Routinely, a solution of 7 μM enzyme in buffer A was used. The azole compound dissolved in DMSO was added in 0.2−3 μL aliquots sequentially to the sample cuvette. The final concentration of DMSO was ≤0.1%. The saturation curves were analyzed using the equation derived from the Hill equation (*29*): $\log[(A - A_0)/(A_\infty - A_0)] = n \log[L] - \log K_d$, where A_0, A_∞, and A are the absorbance of the unligated, ligated, and mixed forms, respectively, measured at the completely shifted Soret positions corresponding to the fractional saturation of the protein capable of binding n molecules of ligand (L).

Crystallization of the FHP_M, FHP_E, and FHP_K Complexes. FlavoHb from *R. eutropha* (20 mg/mL) was crystallized in the presence of a saturating concentration of miconazole, econazole, and ketoconazole (500 μM) with the sitting drop vapor diffusion techniques at 4 and 18 °C. The well solution contained 1.5 M ammonium sulfate, 25% (w/v) glycerol, and 0.1 M Tris (pH 8.5). Brownish crystals that formed within 2 weeks were mounted on a loop and flash-cooled in liquid nitrogen. Crystals of the FHP_M complex belong to monoclinic space group $C2$, while those of the FHP_E and FHP_K complex belong to space group $P4_32_12$, although the crystallization conditions were identical.

Collection of X-ray Diffraction Data, Processing, and Structure Determination. X-ray diffraction data were collected from single crystals for the FHP_M, FHP_E, and FHP_K complexes at the Swiss-Light Source (Villigen, Switzerland). The structures were determined by molecular replacement using the *R. eutropha* flavoHb structure as a search model (PDB entry 1CQX) (*5*). Phase determination was straightforward for the FHP_M complex using EPMR (*30*). In the cases of the FHP_K and FHP_E complexes, only the globin and FAD domains were correctly positioned in the first run using PHASER (*31*). After initial difficulties, the NADH binding domain could be manually modeled into the "omit map" calculated on the basis of the computationally correct positioned part, where the β-sheets of the NADH domain were recognizable just above the noise level. PHASER was also able to localize the NADH domain of one of

Table 1

	FHP_M	FHP_E	FHP_K
	Data Collection		
wavelength (Å)	0.992	0.992	1.001
space group	*C*2	$P4_32_12$	$P4_32_12$
unit cell parameters *a*, *b*, *c* (Å)	121.3, 105.3, 46.4	87.1, 291.3	87.1, 292.2
β (deg)	101.9		
no. of molecules per asymmetric unit	1	2	2
resolution range (Å) (highest-resolution shell)	50.0−2.0 (2.05−2.0)	50.0−2.4 (2.5−2.4)	50.0−2.3 (2.4−2.3)
redundancy	3.1 (2.7)	3.9 (3.7)	4.4 (3.3)
completeness (%)	97.4 (80.3)	99.0 (96.9)	92.7 (67.7)
R_{merge} (%)	7.6 (46.6)	5.1 (54.4)	6.5 (48.3)
$I/\sigma(I)$	13.5 (3.8)	17.1 (3.0)	13.5 (2.6)
	Refinement		
resolution limit (Å)	2.1	2.4	2.3
R_{work}/R_{free} (%)	19.7/23.6 (26.0/30.6)	21.0/24.7 (34.3/42.5)	20.5/24.1 (30.6/35.9)
rms deviation for bond lengths (Å)	0.014	0.013	0.016
rms deviation for bond angles (deg)	1.4	1.5	1.6
average *B* (Å^2)	22.6	26.4	29.1

the two molecules in the asymmetric unit when entered as a separate ensemble. Several cycles of manual rebuilding and refinement were performed using COOT (*32*) and REFMAC5 (*33*). The TLS model was applied because of sizable rigid body vibration of the three domains of the molecules. Models for miconazole, econazole, and ketoconazole were constructed using COOT. Data collection statistics and final refinement parameters are summarized in Table 1. Structural images were generated using PyMol (http://www.pymol.org). Structure factors and final coordinates of the FHP_M, FHP_E, and FHP_K structures are deposited in the PDB as entries 3OZU, 3OZV, and 3OZW, respectively.

RESULTS

Azole Derivatives Bind to Ferric FHP in Solution. Prior to binding studies, purified flavoHb of *R. eutropha* was analyzed for bound phospholipids using thin layer chromatographic methods (Figure S1 of the Supporting Information). Phosphatidylglycerol but not phosphatidylethanolamine could be clearly identified; however, the latter was reported as a major lipid species (*7*). Despite this deviation presumably caused by modified growth conditions, it is important to consider that binding and cocrystallization studies with azole compounds were performed in the presence of the lipid. Attempts to eliminate the lipids lead to precipitation of the *R. eutropha* flavoHb. Binding between the ferric flavoHb and the three azole inhibitors econazole, miconazole, and ketoconazole (Figure 1) was investigated in solution at pH 7 by UV−visible spectroscopy (Figure 2A). The spectral changes of *R. eutropha* flavoHb upon continuous miconazole addition are similar to those observed for *E. coli* flavoHb (*20*). In most cases, the magnitude of the Soret absorption peak is increased, its wavelength shifts from 395 to 414 nm, and the peak at 645 nm disappears. This spectral evolution is characteristic of the conversion of a pentacoordinated to a hexacoordinated ferric heme iron, suggesting that miconazole occupies the sixth iron ligation site. Similar spectra were observed upon titration of *R. eutropha* flavoHb with econazole and ketoconazole, although the wavelength shift is slightly different (Table 2).

The saturation curves of ferric heme from FHP with azole derivatives are shown in Figure 2B. The K_d values for the inhibitors were obtained from the spectral titration curves and are summerized in Table 2. The titration curve with ketoconazole was fitted with the classical one binding site, leading to a K_d value of 10.10 ± 0.07 μM. For econazole and miconazole, titration curves do not fit a hyperbola and were therefore considered as Hill plots. The equilibrium binding constant K_d was determined to 2.6 ± 0.17 and 1.2 ± 0.05 μM for miconazole and econazole, respectively. The K_d values differ substantially in quantitative terms from the published K_i values (*20*), and in addition, the K_d value is lower for econazole than for miconazole and the K_i value vice versa. The discrepancy is to a certain extent comprehensible as the K_d value describes the affinity of lipid-bound flavoHb-Fe(III) for the azole derivatives measured on the basis of the imidazole ligation and the K_i value the inhibition effect of the NOD reaction. The K_d value reflects the affinity of the enzyme for the azole compound prior to the reaction and the K_i value approximately during its turnover. The influence of the lipid on the two processes is presumably different. Thus, the K_d values might decrease in the absence of the lipid as previous studies demonstrate a higher affinity for imidazole binding in a lipid-free A60Y mutant *R. eutropha* flavoHb (*7*).

The sigmoid shape of miconazole and econazole saturation curves was best fitted to the Hill equation with coefficient values, *n*, of 1.74 ± 0.11 and 1.46 ± 0.09, respectively (Table 2), indicating a positive cooperativity. Because a unique binding site was found for either miconazole or econazole, the binding cooperativity does not arise from the binding of multiple inhibitor molecules in the FHP binding site but rather from protein−protein interactions frequently found in heme-containing enzymes and not profoundly understood. It is proposed that the accessibility at low ligand concentrations is decreased by aggregated proteins quantitatively described by Michel (*34*), explaining the physiological binding of oxygen to heme proteins. In previous ligand binding studies conducted with the homologue *Vitreoscilla* Hb (VHB) and in HMP, biphasic equilibrium titration profiles were also found and interpreted as the apparently dimeric nature of the protein (*35*). It is worth noting that crystalline flavoHb of *R. eutropha* reveals a large contact area between the two globin domains of opposing molecules, suggesting that dimerization is at least transiently possible (*28*). Therefore, we propose the aggregation process of flavoHb of *R. eutropha* in

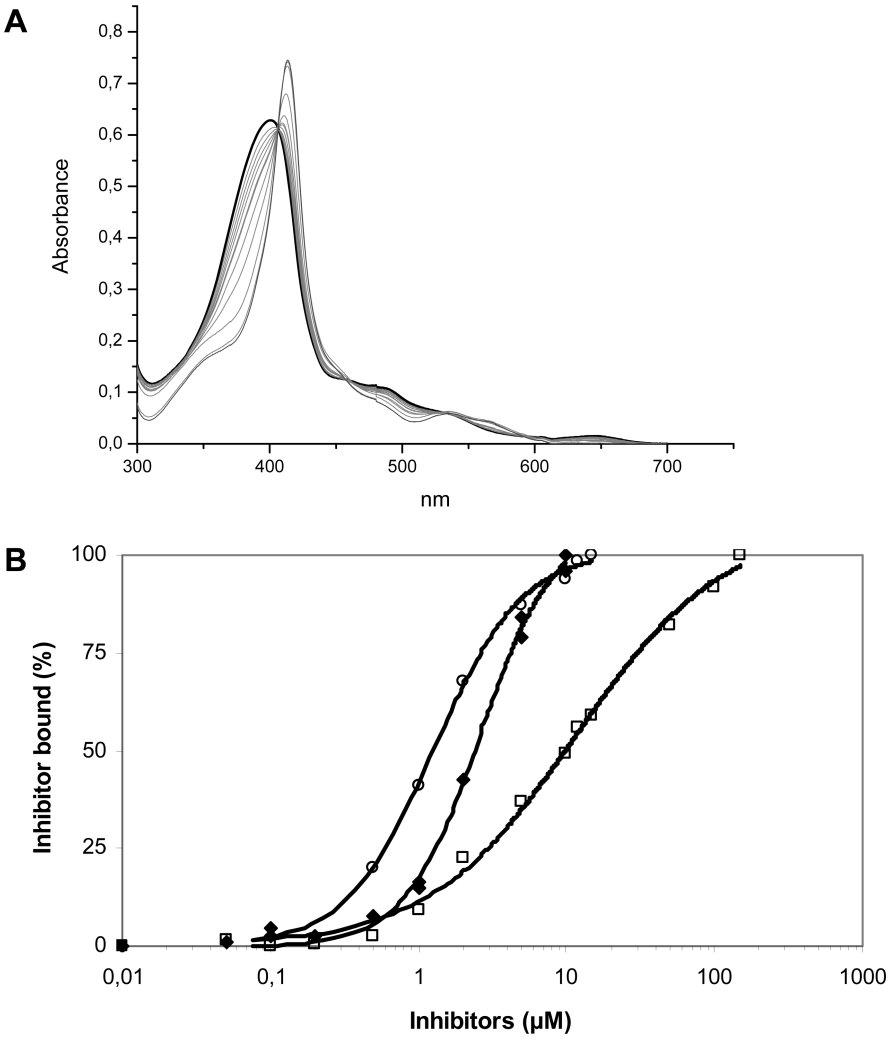

FIGURE 2: Spectrophotometric characterization of ferric *R. eutropha* flavoHb. (A) Titration with miconazole. Spectral changes of the enzyme with increasing miconazole concentrations are shown in the Soret and visible regions. The spectra of the protein without additions, saturated with miconazole, and with intermediate miconazole concentrations are drawn as thin solid, thick solid, and dashed lines, respectively. (B) Saturation curves of three azole derivatives. Increasing concentrations of miconazole (◆), econazole (○), and ketoconazole (□) were added to oxidized flavoHbs (7 μM), and coordination was followed by monitoring the absorbance difference between the inhibitor complex and the free enzyme at 414 nm (miconazole), 414.3 nm (econazole), and 413.2 nm (ketoconazole). Experiments were performed at 22 °C in a solution of 20 mM Tris-HCl buffer and 10 mM KCl (pH 7.5).

Table 2: Absorption Spectroscopic Data and Hill Plot Analyses of the Saturation Curves of Ferric FHP in a Complex with Miconazole, Econazole, or Ketoconazole

axial ligand	absorption maximum (±0.3 nm)	K_d[a] (μM)	n[b]
none	395	–	
miconazole	414	2.60 ± 0.17	1.74 ± 0.11
econazole	414.4	1.28 ± 0.05	1.46 ± 0.09
ketoconazole	413.2	10.10 ± 0.07	

[a]Apparent dissociation constant. [b]Hill coefficient describing the cooperativity of ligand binding.

solution, like those observed for the CYP130 protein in complex with miconazole and econazole (*36*).

Basic Structural Data. The structures of the binary FHP_M, FHP_E, and FHP_K complexes were determined at resolutions of 2.1, 2.4, and 2.3 Å, respectively, which are sufficient to describe the conformation of the inhibitors and their interactions with the polypeptide in detail. Crystallization conditions and crystallographic data are summarized in Table 1. Comparison of the FHP_{Lip}, FHP_M, FHP_E, and FHP_K structures revealed a different orientation of the NADH domain relative to the globin and FAD domains documented by rms deviations of ~0.6 Å for the globin and FAD domains and of ~3.5 Å for the whole FHP (Figure 3A). The rotation of the NADH domain of ~30° implies a more narrow cleft between the FAD and NADH domains in the FHP_E and FHP_K structures ("closed" state) compared to a wider cleft in the FHP_{Lip} and FHP_M structures ("open" state) (Figure 3B). A closed state was previously found in the related HMP structure (*6*). These data substantiate the existence of two distinct positions of the NADH domain in flavoHbs as functionally relevant and not basically as an effect of crystal packing or of sequence variations between proteins of different organisms.

Although the structures of the individual domains are largely conserved, two pronounced local rearrangements that determine the form of the distal heme pocket occur. First, the FHP_{Lip}, FHP_M, FHP_E, and FHP_K complexes contain a distal heme pocket with a volume of ~2000 Å^3 coated by helices A (residues 4−19), B (residues 21−35), E (residues 50−67), G (residues 92−113), and H (residues 116−145). The profile of the pocket is mainly dictated by different positions of helix E. Variations in the range of

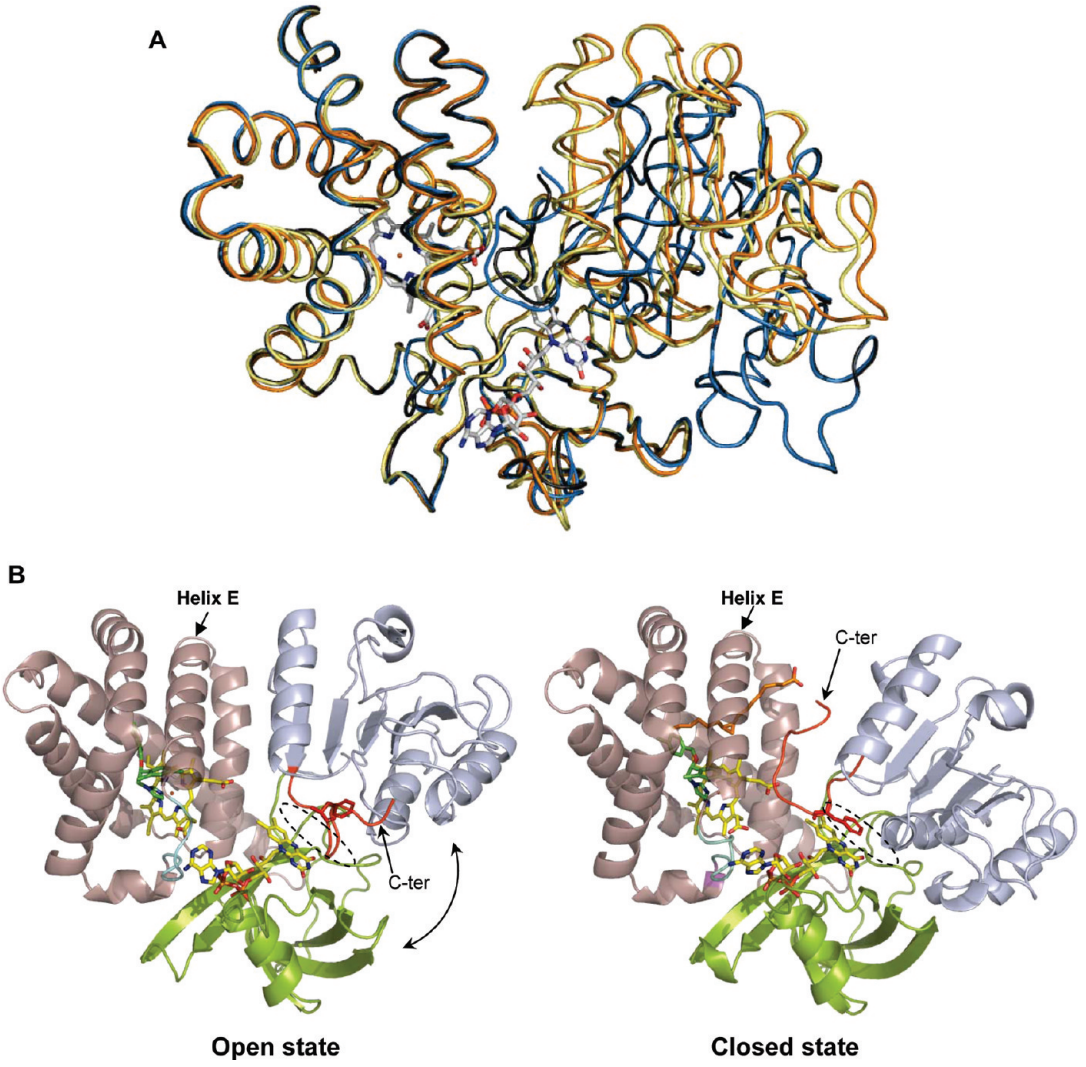

FIGURE 3: (A) Superpositions of the FHP_{Lip} (yellow), FHP_M (orange), FHP_E (blue), and FHP_K (gray) structures. Solely the C_α positions of the globin and FAD domains were applied for alignment. (B) Image of the open FHP_M (left) and closed FHP_E (right) structures. Besides the rearrangement of the NADH domain (light blue) relative to globin and FAD domains (light purple and green, respectively), the C-terminal region (red), helix E (see arrow), and the CE loop (cyan) were subjected to substantial conformational changes. The heme and flavin molecules are colored yellow, and the fatty acid present in FHP_E is colored orange. In the C-terminal region, the Phe396 that forms in FHP_E and FHP_K a stacking interaction with the *re* face of the isoalloxazine ring of FAD is represented as sticks. The dashed circle indicates the approximate position of the NADH binding site that is accessible in the open state and shielded by Phe396 in the closed state.

1.5−4.5 Å are transmitted to helices A and H and, in particular, to the loop between helices C and E (termed 44−52) termed the CE loop that shows differences up to a size of ~7 Å. Conformational alterations are further transferred to the adenosine part of FAD that markedly changes its binding mode and to the loop between the strand of residues 129−224 and the helix of residues 236−244 that flanks FAD. In contrast, no distal heme pocket exists in HMP mainly because of a displacement of helix E of 9 Å toward heme (*6*). Second, the C-terminal region (residues 394−403) of the enzyme located in front of the C-terminal side of the central β-sheet of the NADH domain in the open FHP_{lip} and FHP_M structures moves toward the interface of the three domains in the closed FHP_E and FHP_K structures because of the rigid-body motion of the NADH domain. As a result, the C-terminal region becomes part of the distal heme pocket in the closed state and enhances its interactions with FAD in comparison to those in the open state (Figure 3B, right).

Azole Conformations and Protein−Azole Interactions. The azole inhibitors are unambiguously identifiable in the distal heme pocket of the FHP_M, FHP_E, and FHP_K structures (illustrated for miconazole in Figure 4A). The di- or monochlorophenylmethoxy groups of miconazole and econazole and the dichlorophenyl groups of ketoconazole are deeply embedded inside the pocket and, hence, termed inner substituents, whereas the dichlorophenyl and dioxolan-methoxyphenyl-piperazine-acetyl groups point to the entrance of the pocket termed outer substituents. The corresponding binding sites are called inner and outer sites; that of imidazole lies between them. The three substituents of the azole compounds are in contact with heme *b*. In comparison to the position of the phospholipid (phosphatidylethanolamine identified) in the FHP_{Lip} crystal structure (*7*), the position of the imidazole substituent approximately coincides with its cyclomethylene group, and the inner and outer substituents coincide with the *sn*-1 and *sn*-2 fatty acid chains (Figure 4B). The U-shaped fatty acid chains of the phospholipid somehow encircle the aromatic substituents and the dioxolane ring of ketoconazole.

The azole inhibitors are ligated to the heme iron via the imidazole N1 atom, in agreement with the UV−visible spectroscopic data (Figure 2), and the distance is ~2.1 Å for miconazole,

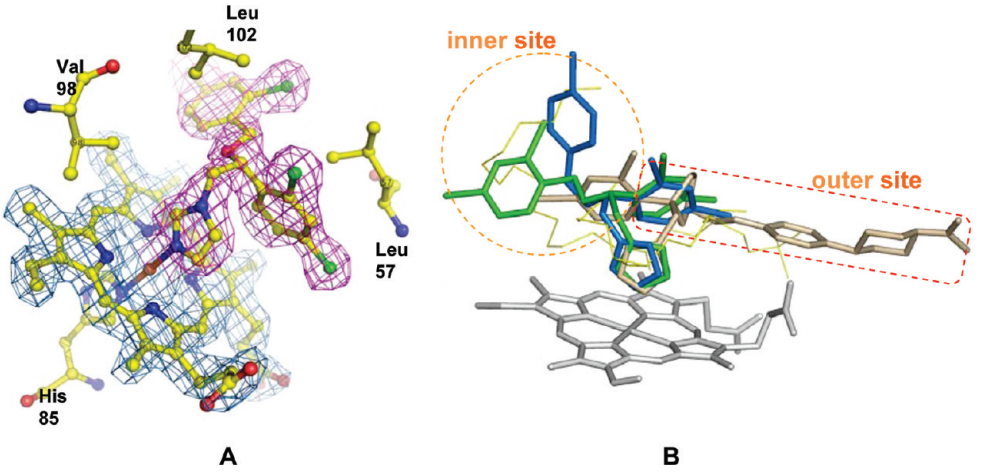

FIGURE 4: (A) Structure of miconazole at its binding site. The electron density of the heme group and miconazole is colored blue and purple, respectively (contour level of 1.5σ). In agreement with spectroscopic data, the imidazole nitrogen of miconazole is coordinated to the heme iron. (B) Superimposed miconazole (green), econazole (blue), ketoconazole (wheat), and phosphoplipid (thin yellow line). The alignment is based on the C_α coordinates of the globin and FAD domains of the FHP_M, FHP_E, FHP_K, and FHP_{Lip} structures. The inner and outer sites (detailed in the text) are surrounded with dashed lines.

econazole, and ketoconazole. The imidazole ring is oriented roughly perpendicular to the porphyrin macrocycle (Figure 4B). The N1 atom occupies the sixth coordination site of the iron and is thus in line to the proximal imidazole nitrogen of His85. While the heme iron is shifted ~0.2 Å out of the porphyrin plane toward His85 in the FHP_{Lip} structure, the iron moves into the plane and the distance to the two imidazole nitrogens becomes equidistant (Figure 4A). Econazole compared to miconazole is rotated ~5° around the branching carbon atom (the rotation axis being perpendicular to the heme plane), implying an equivalent counterclockwise movement of the imidazole ring to ensure iron ligation. Both azole compounds are present in a conformation in which the imidazole and dichlorophenyl rings are within van der Waals distance of each other and sandwiched between Phe43 and Leu57. Phe28, Tyr29, and Val98 shield the imidazole ring from the back side (Figure 5). The inner dichlorophenylmethoxy substituent of miconazole points in the opposite direction compared to the other rings and does not contact them. Its aromatic ring is sandwiched between Leu102 and a compound whose nature could not be derived from the electron density shape.

The monochlorophenylmethoxy group of econazole is only weakly observed in the conformation of the inner substituent of miconazole. It is highly occupied in a conformation where the aromatic ring is rotated ~140° toward the other two rings and sandwiched between Leu57 and Leu102. Econazole in this more compact conformation creates space in the inner site that appears to be occupied by a phospholipid. However, interpretable electron density is visible for only a fraction of the original phosphatidylglycerol and modeled as a fatty acid. We do not know whether its major part is flexible or becomes hydrolyzed. The fatty acid partly overlaps with the end of the *sn*-1 fatty acid chain of the phospholipid found in the FHP_{Lip} structure and is surrounded by various hydrophobic side chains, including Val61, Ala63, Leu74, Val77, Ile81, Leu129, Trp122, Tyr126, and the dichloromethoxy and heme groups.

In the FHP_K structure, the dichlorophenyl, imidazole, and dioxolane rings of ketoconazole are in mutual contact; the aromatic rings are nearly staggered with respect to each other, and the dioxolane ring is roughly perpendicular to them. Compared to the other two azole inhibitors, ketoconazole is shifted 3 Å parallel to the heme porphyrin plane toward the

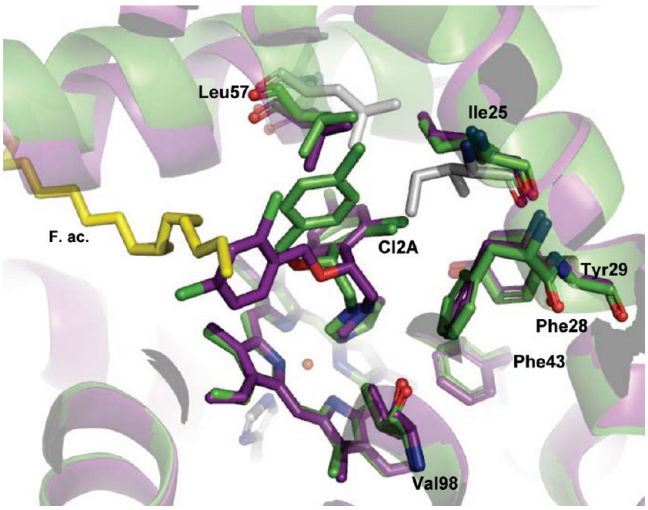

FIGURE 5: Binding of miconazole (purple) and econazole (green) focusing on the inner site. The di- and monochlorophenylmethoxy groups of miconazole and econazole are differently positioned. The aromatic rings are rotated ~140° compared to each other, which creates space in the inner site of the FHP_E complex. The electron density extending from the inner site to the NADH domain was modeled as a fatty acid (orange). The positions of Leu57 and Ile25 in the FHP_{Lip} structure are colored gray.

pocket entrance, implying that the ligated imidazole points from a different direction toward the heme iron (Figure 4B) and the dichlorophenyl group is shifted away from the inner site. The available space is occupied by the phospholipid fragment in one molecule of the asymmetric unit; in the second, the electron density of the fatty acid and also the ketoconazole is less defined. The elongated outer substituent of ketoconazole extends to the pocket entrance and contacts FAD.

The three azole derivatives, in particular the chlorine atoms, form a series of van der Waals contacts with the polypeptide. For example, in FHP_M, the dichlorophenyl chlorides are surrounded by Ile25, Phe28, Ala56, Leu57, and Leu102 and the dichlorophenylmethoxy chlorides by Leu17, Leu57, Val61, Leu102, Trp122, Ala125, Tyr126, and Leu129. Detailed structural data about protein−azole interactions are so far only described for cytochrome P450 enzymes (*37*). The distal heme pocket in FHP and

cytochrome P450 enzymes share high hydrophobicity and an extended size that are basic prerequisites for binding the bulky and rather nonpolar azole compounds. However, the global architecture of the enzymes, the conformation of the azole compounds, and all interactions are different such that FHP provides a second independent system for studying the binding of azole inhibitors established as important drugs for fungal infections. Interestingly, the cytochrome P450−azole interface is also characterized by multiple interactions with chlorine atoms but involves to a larger extent aromatic side chains.

Specific changes in the distal heme pocket upon phospholipid and/or inhibitor binding can be described on the basis of the discrimination of an open and closed enzyme state. The heme pockets of the open FHP_{Lip} and FHP_M complexes are surprisingly similar (considering the drastic structural differences between the phospholipid and miconazole). Solely local changes occur. Upon phospholipid to miconazole exchange, helices A, G, and E are shifted by only ~1.0, ~0.7, and ~1.3 Å, respectively, toward and helix B that is ~0.5 Å from the pocket, resulting in a small net shrinkage of the pocket of FHP_M compared to FHP_{Lip} (Figure 6A). The largest side chain rearrangements are related to Leu57 of helix E, which shifts 3.3 Å toward the dichlorophenyl ring, and Ile25 of helix B, which moves 4.5 Å out of the pocket to evade chlorine Cl2A (Figure 5).

Substantial global and local conformational changes occur when the open and closed binary complexes are compared. At their C-terminal end, helix E is rotated outward in the closed FHP_E and FHP_K (Figure 6) compared to the open FHP_{Lip} and FHP_M structures, thereby creating a pore between helices E and F. This pore allows the passage of the phospholipid fragment that extends from the inner substituent of econazole and ketoconazole to the bulk solvent close to the NADH domain. Notably, the position of the found fatty acid fragment would interfere with the NADH domain of the open state, especially with Glu388. The rotation of the N-terminal end of helix E (adjacent to the pocket entrance) and the induced rearrangement of the CE loop result in an encapsulation of the active site in the FHP_E structure, while the azole compound in the FHP_M remains accessible for bulk solvent. The CE loop of the FHP_E (Figure 6B) compared to the FHP_M (Figure 6A) structure is characterized by an extra helix turn and an increased conformational flexibility. As a result, the imidazole group of His47 located in the middle of the CE loop is directed toward the solvent in FHP_{Lip} and FHP_M and rotated toward the protein interior (shift of 6.9 Å) in the FHP_E structure. These rearrangements also influence the conformation of Tyr29 and Gln53, both identified as catalytically relevant for substrate stabilization (*38*, *39*). Tyr29 and Gln53 are within van der Waals distance of the imidazole and dichlorophenyl rings of econazole and hydrogen-bonded to each other, the latter also to His47, suggesting that the outer site geometry of the FHP_E structure resembles the active site geometry prior to the chemical reaction. These residues might form hydrogen bonds and/or serve as proton donors during the chemical reaction. In contrast to the open FHP_M and FHP_{Lip} structures, the closed FHP_E and FHP_K structures use the C-terminal arm as part of the substrate binding site that might be crucial for forming a functional active site. The proximity between the C-terminal arm and the CE loop in FHP_E (the shortest distance of 4.2 Å being between His47 and Pro398) might influence their conformations. Moreover, a weak van der Waals contact exists between the most exposed C4 chlorine atom of the outer substituent and Pro398 of the C-terminal segment in the FHP_E structure. Because of the immense space requirements

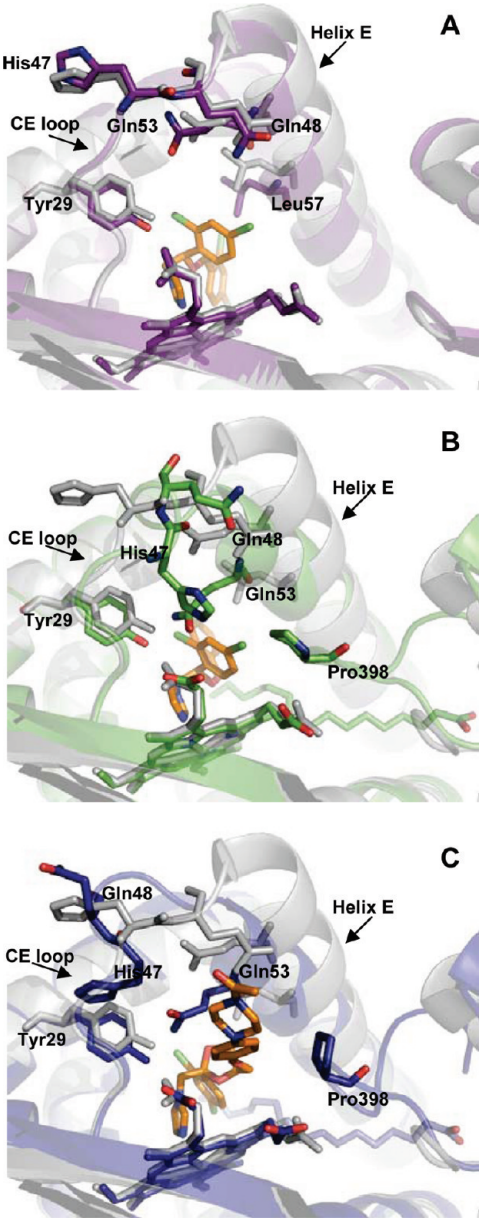

FIGURE 6: Distal heme pocket of FHP_M (A), FHP_E (B), and FHP_K (C) viewed from the entrance. The azole compounds are colored orange. For comparison, the structure of FHP_{Lip} is colored gray. In FHP_E (and FHP_K, to a lesser extent), helix E and the CE loop (arrows) undergo rearrangements that induce repositioning of Glu53, His47, and Tyr29, yielding a "catalytically active-like" geometry.

of the outer substituent of ketoconazole, the FHP_E and FHP_K structures differ in the outer site of the heme pocket mainly by local conformational changes of the CE loop and the C-terminal arm (Figure 6B,C). His47, Gln48, and Pro398, pointing toward the pocket in the FHP_E structure, are turned away in the FHP_K structure. Therefore, the outer substituent of ketoconazole is accessible from bulk solvent and not encapsulated as econazole in the FHP_E structure.

DISCUSSION

Consequences of Ligand-Induced Open and Closed States for the Reaction Cycle. The structures of *R. eutropha* flavoHb in complexes with three azole compounds indicated the existence of an open and a closed state (adjusted by the absence or presence and the nature of the ligand in the distal heme pocket) characterized

by a rigid body motion of the NADH domain accompanied by conformational changes in the C-terminal arm. These results substantiate the existence of two major states in flavoHbs previously suggested from heterogeneous kinetic data and from the comparison between the *E. coli* and *R. eutropha* flavoHb structures (*6*, *39*, *40*).

In the closed HMP structure, helix E is attached to heme *b*, allowing the formation of a contact area between helix E of the globin domain and the C-terminal arm of the NADH domain. In comparison, the open state might be unfavorable because helix E in the conformation attached to heme *b* and the core of the NADH domain are too far from each other to form an interdomain interaction. In the open FHP_{Lip} structure, the voluminous phospholipid pushes helix E toward the NADH domain such that a contact between helix E and the core of the NADH domain is feasible. The formation of an interdomain hydrogen bond network among Arg59, Asn67, Arg375, His378, Asp379, Lys382, and Glu388, several solvent molecules, and the phosphate of the lipid might stabilize the open state. More importantly, the phosphate of the phospholipid would collide with the C-terminal arm in the position of the closed state (Figure 3B). The FHP_M structure was also found in the open state, although no phospholipid is present, such that the existence of a closed state under appropriate conditions cannot be excluded. The FHP_E and FHP_K structures are present in a closed state despite the described large displacement of helix E. This surprising finding can be rationalized on the basis of the observed different positions of the inner substituents that allow in FHP_E and FHP_K, but not in FHP_M, the binding of a lipid fragment that would collide with the NADH domain in the open state (Figure 3B). Comparison of the FHP_E and FHP_M structures also offers an explanation for why econazole but not miconazole binding allows the binding of a lipid fragment. In the more occupied conformation of the chlorinated phenyl group found in FHP_E, the extra chlorine atom of miconazole would interfere with the lipid and thus impair its binding (Figure 5).

Although the binary flavoHb−azole inhibitor structures cannot provide direct mechanistic clues, a detailed analysis of the two states shed some light on the catalytic cycle of flavoHbs. First, in the closed state, the C-terminal arm shields the isoalloxazine ring from bulk solvent as the aromatic side chains of Phe396 face the pyrazine ring of FAD at the potential nicotinamide binding site (Figure 3B). The rearrangement of the C-terminal arm in the open state makes the *re* side of the isoalloxazine ring accessible for solvent, although a perfect coplanar binding of the bulky nicotinamide ring of NADH still requires conformational changes especially of the Thr357 and Val395 side chains. The conformational flexibility of the C-terminal region might be a tool for controlling the access to the isoalloxazine ring for NADH, which appears to be favored in the open state. In the structurally related ferredoxin-$NAD(P)^+$ reductase, productive NADH binding requires the displacement of the C-terminal tyrosine side chain (*41*, *42*) that stacks with the isoalloxazine ring in many members of the "FNR family" (*43*), including CytP450 reductase and sulfite reductase (*44*, *45*). Second, the surroundings of FAD and heme *b* and of the intervening region between the prosthetic groups (including the positions of Lys84, Glu394, and the bridging solvent molecule) differ in the open and closed states because of the differently positioned C-terminal region. However, the relative positions of the prosthetic groups remained unchanged, suggesting that, at a distance of ~6.3 Å, the electron transfer rate should not be largely affected. Third, the different conformations of the C-terminal arm and helix E cause an accessible heme pocket in the open state and a largely encapsulated one in the closed state. In the closed state of the FHP_E structure, the pocket is shrunken and the catalytically crucial residues Gln53 and Tyr29 are closer to the heme iron. These findings allowed us to postulate a preliminary mechanism involving open-to-closed transition processes induced by substrate and NADH binding. At first, the substrate and NADH bind to the open state. NADH transfers a hydride ion to FAD, which is reoxidized by a stepwise electron transfer to the heme iron and the substrate. NAD^+ is released; a subsequent open-to-closed transition event forms the active site, and the reaction begins. After product formation, the protein returns to the open state.

Suitability of FlavoHbs as Drug Targets. FlavoHbs play a vital role in NO detoxification in a variety of human and plant pathogens, including *Salmonella enterica*, *Pseudomonas aeruginosa*, *Mycobacterium tuberculosis*, and *Erwina chrysanthemi*, and have therefore been discussed as attractive targets for antibiotic agents. Azole derivatives composed of an imidazole bearing bulky aromatic substituents (Figure 1) are considered as promising inhibitors because of their capability to ligate to heme and to multiply interact with the hydrophobic distal heme pocket. Gardner's group substantiated this idea by inhibition studies on *E. coli*, *R. eutropha*, *Candida albicans*, and *Saccharomyces cerevisiae* flavoHbs with respect to NOD activity (*3*, *20*). The presented X-ray structures of the FHP_M, FHP_E, and FHP_K complexes provided the basis for understanding azole binding on atomic grounds and designing novel inhibitors with increased affinity.

An analysis of the known flavoHb structures reveals a high plasticity of the distal heme pocket mainly because of the conformational flexibility of helix E, the CE loop, and various large aliphatic side chains. In contrast to many other proteins in which the substrate binding site is not significantly changed upon ligand binding, drastic conformational changes become visible at the distal heme pocket in flavoHbs to allow an individual optimization of the polypeptide−ligand interactions. Remarkably, the pocket can bind both the *sn*-1 and *sn*-2 chains of the phospholipid and the different bulky N1 substituents of the azole derivatives. Despite this ligand-induced adaptation of the polypeptide scaffold, the inner site is still too voluminous for the chlorinated phenylmethoxy substituents documented by the two binding conformations of the aromatic ring (Figure 4B). An inhibitor consisting of a bicyclic ring system or bulky phenyl ring substituents could be consequently constructed to potentially increase the number of interactions. The inner substituent might also be enlarged via replacement of a chlorine atom with an elongated aliphatic chain that mimics the phospholipid in the FHP_E and FHP_K structures. Phospholipid binding should be thus prevented, and a sufficiently long substituent might disrupt the essential open-to-closed transition process. The less globular outer site expands toward the pocket entrance and is completely filled out by ketoconazole in the FHP_K structure. Its hydrophobic character is less pronounced compared to that of the inner site and creates the possibility of designing specific hydrogen bonds. It would be also challenging to further elongate the outer substituent of ketoconazole with the aim of impairing FAD binding. Both the elimination of FAD and the disruption of the open-to-closed transition process open new perspectives for the development of inhibitors, in particular, as according to kinetic data (*20*) azole compounds cannot compete with O_2 for heme ligation in the ferrous iron state and thus do not directly inhibit

the redox reaction. According to kinetic data (*20*), azole derivatives hamper the flow of electrons between NADH and the heme iron, which is consistent with the presented structural data. Possibly, the azole derivatives stabilize a state with low NADH affinity that is compatible with the slower FAD reduction kinetics attributed to a lower rate of hydride transfer and would explain the increased level of inhibition of azole compounds as a consequence of a decreased NADH availability (*20*).

Despite the described promising prospects, a rational design of the suitable (azole) inhibitors is intricate because of the competition between the phospholipid and the inhibitor for the binding site and the consideration of two states; both aspects are interconnected and influence the pocket properties.

ACKNOWLEDGMENT

We thank Hartmut Michel for continuous support and the staff of the PXII beamline at the Swiss-Light-Source in Villigen, Switzerland, for help during data collection. We thank Florence Lederer and Tania Bizouarn for helpful discussions.

SUPPORTING INFORMATION AVAILABLE

Prior to binding studies, purified flavoHb of *R. eutropha* was analyzed for bound phospholipids using the TLC method. This material is available free of charge via the Internet at http://pubs.acs.org.

REFERENCES

1. Poole, R. K., and Hughes, M. N. (2000) New functions for the ancient globin family: Bacterial responses to nitric oxide and nitrosative stress. *Mol. Microbiol. 36*, 775–783.
2. Bonamore, A., and Boffi, A. (2008) Flavohemoglobin: Structure and reactivity. *IUBMB Life 60*, 19–28.
3. Gardner, P. R. (2005) Nitric oxide dioxygenase function and mechanism of flavohemoglobin, hemoglobin, myoglobin and their associated reductases. *J. Inorg. Biochem. 99*, 247–266.
4. Frey, A. D., and Kallio, P. T. (2003) Bacterial hemoglobins and flavohemoglobins: Versatile proteins and their impact on microbiology and biotechnology. *FEMS Microbiol. Rev. 27*, 525–545.
5. Ermler, U., Siddiqui, R. A., Cramm, R., and Friedrich, B. (1995) Crystal structure of the flavohemoglobin from *Alcaligenes eutrophus* at 1.75 Å resolution. *EMBO J. 14*, 6067–6077.
6. Ilari, A., Bonamore, A., Farina, A., Johnson, K. A., and Boffi, A. (2002) The X-ray structure of ferric *Escherichia coli* flavohemoglobin reveals an unexpected geometry of the distal heme pocket. *J. Biol. Chem. 277*, 23725–23732.
7. Ollesch, G., Kaunzinger, A., Juchelka, D., Schubert-Zsilavecz, M., and Ermler, U. (1999) Phospholipid bound to the flavohemoprotein from *Alcaligenes eutrophus*. *Eur. J. Biochem. 262*, 396–405.
8. Tarricone, C., Galizzi, A., Coda, A., Ascenzi, P., and Bolognesi, M. (1997) Unusual structure of the oxygen-binding site in the dimeric bacterial hemoglobin from *Vitreoscilla* sp. *Structure 5*, 497–507.
9. Bonamore, A., Farina, A., Gattoni, M., Schinina, M. E., Bellelli, A., and Boffi, A. (2003) Interaction with membrane lipids and heme ligand binding properties of *Escherichia coli* flavohemoglobin. *Biochemistry 42*, 5792–5801.
10. Cruz-Ramos, H., Crack, J., Wu, G., Hughes, M. N., Scott, C., Thomson, A. J., Green, J., and Poole, R. K. (2002) NO sensing by FNR: Regulation of the *Escherichia coli* NO-detoxifying flavohaemoglobin, Hmp. *EMBO J. 21*, 3235–3244.
11. Bodenmiller, D. M., and Spiro, S. (2006) The yjeB (nsrR) gene of *Escherichia coli* encodes a nitric oxide-sensitive transcriptional regulator. *J. Bacteriol. 188*, 874–881.
12. Gilberthorpe, N. J., and Poole, R. K. (2008) Nitric oxide homeostasis in *Salmonella typhimurium*: Roles of respiratory nitrate reductase and flavohemoglobin. *J. Biol. Chem. 283*, 11146–11154.
13. Gardner, A. M., Martin, L. A., Gardner, P. R., Dou, Y., and Olson, J. S. (2000) Steady-state and transient kinetics of *Escherichia coli* nitric-oxide dioxygenase (flavohemoglobin). The B10 tyrosine hydroxyl is essential for dioxygen binding and catalysis. *J. Biol. Chem. 275*, 12581–12589.
14. Gardner, P. R., Gardner, A. M., Martin, L. A., and Salzman, A. L. (1998) Nitric oxide dioxygenase: An enzymic function for flavohemoglobin. *Proc. Natl. Acad. Sci. U.S.A. 95*, 10378–10383.
15. Hausladen, A., Gow, A. J., and Stamler, J. S. (1998) Nitrosative stress: Metabolic pathway involving the flavohemoglobin. *Proc. Natl. Acad. Sci. U.S.A. 95*, 14100–14105.
16. Gardner, P. R. (2008) Assay and characterization of the NO dioxygenase activity of flavohemoglobins. *Methods Enzymol. 436*, 217–237.
17. Gardner, A. M., Gessner, C. R., and Gardner, P. R. (2003) Regulation of the nitric oxide reduction operon (norRVW) in *Escherichia coli*. Role of NorR and sigma54 in the nitric oxide stress response. *J. Biol. Chem. 278*, 10081–10086.
18. Kim, S. O., Orii, Y., Lloyd, D., Hughes, M. N., and Poole, R. K. (1999) Anoxic function for the *Escherichia coli* flavohaemoglobin (Hmp): Reversible binding of nitric oxide and reduction to nitrous oxide. *FEBS Lett. 445*, 389–394.
19. Bonamore, A., Gentili, P., Ilari, A., Schinina, M. E., and Boffi, A. (2003) *Escherichia coli* flavohemoglobin is an efficient alkylhydroperoxide reductase. *J. Biol. Chem. 278*, 22272–22277.
20. Helmick, R. A., Fletcher, A. E., Gardner, A. M., Gessner, C. R., Hvitved, A. N., Gustin, M. C., and Gardner, P. R. (2005) Imidazole antibiotics inhibit the nitric oxide dioxygenase function of microbial flavohemoglobin. *Antimicrob. Agents Chemother. 49*, 1837–1843.
21. Nobre, L. S., Todorovic, S., Tavares, A. F., Oldfield, E., Hildebrandt, P., Teixeira, M., and Saraiva, L. M. (2010) Binding of azole antibiotics to *Staphylococcus aureus* flavohemoglobin increases intracellular oxidative stress. *J. Bacteriol. 192*, 1527–1533.
22. Akins, R. A. (2005) An update on antifungal targets and mechanisms of resistance in *Candida albicans*. *Med. Mycol. 43*, 285–318.
23. Seward, H. E., Roujeinikova, A., McLean, K. J., Munro, A. W., and Leys, D. (2006) Crystal structure of the *Mycobacterium tuberculosis* P450 CYP121-fluconazole complex reveals new azole drug-P450 binding mode. *J. Biol. Chem. 281*, 39437–39443.
24. Podust, L. M., Poulos, T. L., and Waterman, M. R. (2001) Crystal structure of cytochrome P450 14α-sterol demethylase (CYP51) from *Mycobacterium tuberculosis* in complex with azole inhibitors. *Proc. Natl. Acad. Sci. U.S.A. 98*, 3068–3073.
25. Cupp-Vickery, J. R., Garcia, C., Hofacre, A., and McGee-Estrada, K. (2001) Ketoconazole-induced conformational changes in the active site of cytochrome P450eryF. *J. Mol. Biol. 311*, 101–110.
26. Zhao, Y., White, M. A., Muralidhara, B. K., Sun, L., Halpert, J. R., and Stout, C. D. (2006) Structure of microsomal cytochrome P450 2B4 complexed with the antifungal drug bifonazole: Insight into P450 conformational plasticity and membrane interaction. *J. Biol. Chem. 281*, 5973–5981.
27. Ahmad, Z., Sharma, S., and Khuller, G. K. (2006) Azole antifungals as novel chemotherapeutic agents against murine tuberculosis. *FEMS Microbiol. Lett. 261*, 181–186.
28. Ermler, U., Siddiqui, R. A., Cramm, R., Schroder, D., and Friedrich, B. (1995) Crystallization and preliminary X-ray diffraction studies of a bacterial flavohemoglobin protein. *Proteins 21*, 351–353.
29. Brault, D., and Rougee, M. (1974) Binding of imidazole and 2-methylimidazole by hemes in organic solvents. Evidence for five-coordination. *Biochem. Biophys. Res. Commun. 57*, 654–659.
30. Kissinger, C. R., Gehlhaar, D. K., and Fogel, D. B. (1999) Rapid automated molecular replacement by evolutionary search. *Acta Crystallogr. D55*, 484–491.
31. McCoy, A. J., Grosse-Kunstleve, R. W., Adams, P. D., Winn, M. D., Storoni, L. C., and Read, R. J. (2007) Phaser crystallographic software. *J. Appl. Crystallogr. 40*, 658–674.
32. Emsley, P., Lohkamp, B., Scott, W. G., and Cowtan, K. (2010) Features and development of Coot. *Acta Crystallogr. D66*, 486–501.
33. Vagin, A. A., Steiner, R. A., Lebedev, A. A., Potterton, L., McNicholas, S., Long, F., and Murshudov, G. N. (2004) REFMAC5 dictionary: Organization of prior chemical knowledge and guidelines for its use. *Acta Crystallogr. D60*, 2184–2195.
34. Michel, D. (2007) Cooperative equilibrium curves generated by ordered ligand binding to multi-site molecules. *Biophys. Chem. 129*, 284–288.
35. Bolognesi, M., Boffi, A., Coletta, M., Mozzarelli, A., Pesce, A., Tarricone, C., and Ascenzi, P. (1999) Anticooperative ligand binding properties of recombinant ferric *Vitreoscilla* homodimeric hemoglobin: A thermodynamic, kinetic and X-ray crystallographic study. *J. Mol. Biol. 291*, 637–650.
36. Ouellet, H., Podust, L. M., and de Montellano, P. R. (2008) *Mycobacterium tuberculosis* CYP130: Crystal structure, biophysical characterization, and interactions with antifungal azole drugs. *J. Biol. Chem. 283*, 5069–5080.

37. Strushkevich, N., Usanov, S. A., and Park, H. W. (2010) Structural basis of human CYP51 inhibition by antifungal azoles. *J. Mol. Biol. 397*, 1067–1078.
38. Bonamore, A., Chiancone, E., and Boffi, A. (2001) The distal heme pocket of *Escherichia coli* flavohemoglobin probed by infrared spectroscopy. *Biochim. Biophys. Acta 1549*, 174–178.
39. Mukai, M., Mills, C. E., Poole, R. K., and Yeh, S. R. (2001) Flavohemoglobin, a globin with a peroxidase-like catalytic site. *J. Biol. Chem. 276*, 7272–7277.
40. Gardner, P. R., Gardner, A. M., Martin, L. A., Dou, Y., Li, T., Olson, J. S., Zhu, H., and Riggs, A. F. (2000) Nitric-oxide dioxygenase activity and function of flavohemoglobins. Sensitivity to nitric oxide and carbon monoxide inhibition. *J. Biol. Chem. 275*, 31581–31587.
41. Tejero, J., Perez-Dorado, I., Maya, C., Martinez-Julvez, M., Sanz-Aparicio, J., Gomez-Moreno, C., Hermoso, J. A., and Medina, M. (2005) C-terminal tyrosine of ferredoxin-$NADP^+$ reductase in hydride transfer processes with $NAD(P)^+$/H. *Biochemistry 44*, 13477–13490.
42. Peregrina, J. R., Sanchez-Azqueta, A., Herguedas, B., Martinez-Julvez, M., and Medina, M. (2010) Role of specific residues in coenzyme binding, charge-transfer complex formation, and catalysis in *Anabaena* ferredoxin $NADP^+$-reductase. *Biochim. Biophys. Acta 1797*, 1638–1646.
43. Karplus, P. A., Daniels, M. J., and Herriott, J. R. (1991) Atomic structure of ferredoxin-$NADP^+$ reductase: Prototype for a structurally novel flavoenzyme family. *Science 251*, 60–66.
44. Wang, M., Roberts, D. L., Paschke, R., Shea, T. M., Masters, B. S., and Kim, J. J. (1997) Three-dimensional structure of NADPH-cytochrome P450 reductase: Prototype for FMN- and FAD-containing enzymes. *Proc. Natl. Acad. Sci. U.S.A. 94*, 8411–8416.
45. Gruez, A., Pignol, D., Zeghouf, M., Coves, J., Fontecave, M., Ferrer, J. L., and Fontecilla-Camps, J. C. (2000) Four crystal structures of the 60 kDa flavoprotein monomer of the sulfite reductase indicate a disordered flavodoxin-like module. *J. Mol. Biol. 299*, 199–212.
46. Wishart, D. S., Knox, C., Guo, A. C., Shrivastava, S., Hassanali, M., Stothard, P., Chang, Z., and Woolsey, J. (2006) DrugBank: A comprehensive resource for in silico drug discovery and exploration. *Nucleic Acids Res. 34*, D668–D672.
47. Wishart, D. S., Knox, C., Guo, A. C., Cheng, D., Shrivastava, S., Tzur, D., Gautam, B., and Hassanali, M. (2008) DrugBank: A knowledgebase for drugs, drug actions and drug targets. *Nucleic Acids Res. 36*, D901–D906.